Structure, Vol. 13, 873–882, June, 2005, ©2005 Elsevier Ltd All rights reserved. DOI 10.1016/j.str.2005.03.013

Structural Dissection of ATP Turnover in the Prototypical GHL ATPase TopoVI

Kevin D. Corbett and James M. Berger*
Department of Molecular and Cellular Biology
227 Hildebrand Hall 3206
University of California, Berkeley
Berkeley, California 94720

Summary

GHL proteins are functionally diverse enzymes defined by the presence of a conserved ATPase domain that self-associates to trap substrate upon nucleotide binding. The structural states adopted by these enzymes during nucleotide hydrolysis and product release, and their consequences for enzyme catalysis, have remained unclear. Here, we have determined a complete structural map of the ATP turnover cycle for topoVI-B, the ATPase subunit of the archaeal GHL enzyme topoisomerase VI. With this ensemble of structures, we show that significant conformational changes in the subunit occur first upon ATP binding, and subsequently upon release of hydrolyzed P_i. Together, these data provide a structural framework for understanding the role of ATP hydrolysis in the type II topoisomerase reaction. Our results also suggest that the GHL ATPase module is a molecular switch in which ATP hydrolysis serves as a prerequisite but not a driving force for substrate-dependent structural transitions in the enzyme.

Introduction

GHKL ATPases are a broad family of enzymes with widely varying cellular functions found throughout prokaryotes and eukaryotes (Bergerat et al., 1997; Dutta and Inouye, 2000). The name of the family is derived from four archetypal members: DNA gyrase B (GyrB), the ATPase subunit of a type II topoisomerase (topo); heat shock protein 90 (Hsp90), a molecular chaperone; the CheA histidine kinase, part of the bacterial two-component signaling pathway; and MutL, a component of the conserved MutSLH DNA mismatch repair system (Dutta and Inouye, 2000). The hallmark of a GHKL protein is its ATPase domain (termed the GHKL domain), which is unrelated to other canonical ATP binding folds, such as Walker-type ATPases or serine/threonine kinases.

Three of the four founding members of the GHKL ATPase family, including the type II topos, Hsp90 and MutL, comprise a distinct subfamily of enzymes, termed "GHL" proteins, that are structurally and functionally distinct from the histidine kinases. These enzymes exist as homodimers or A_2B_2 heterotetramers and exhibit a similar overall domain organization, in which the N-terminal GHKL domain is followed by a second conserved domain that also forms part of the ATP binding site. This bipartite module is in turn linked to a C-terminal dimerization domain that is functionally important and different in each subfamily (Figure 1).

Upon binding nucleotide, the two GHKL domains of an enzyme self-associate (Ban and Yang, 1998; Wigley et al., 1991), forming an ATP-actuated "gate" that helps capture a substrate molecule within an internal cavity in the enzyme. When ATP binds, its γ-phosphate is liganded by a glycine-rich loop, termed the "ATP lid," that is reminiscent, both in structure and function, of the P loop motifs of other ATPase families (Ban and Yang, 1998; Prodromou et al., 1997a; Wigley et al., 1991). In all GHL proteins, with the possible exception of Hsp90 (Prodromou et al., 2000), the ATP lid of each GHKL domain and its association with bound nucleotide is stabilized through contacts with an N-terminal extension, termed the "strap," which is provided by the dimer mate. This configuration creates an entwined structure in which both the active site architecture and ATP hydrolysis activity are dependent on GHKL domain dimerization (Ban et al., 1999; Wigley et al., 1991).

The second conserved domain shared by GHL family members, referred to as the "transducer" domain, is peripherally involved in nucleotide binding. One segment from the transducer domain, termed the "switch loop," extends into the ATP binding site and positions a basic residue (lysine in type II topos and MutL, and arginine in Hsp90) close to the γ-phosphate of bound ATP (Ban et al., 1999; Meyer et al., 2003; Wigley et al., 1991). In all three GHL enzymes, this basic residue has been shown biochemically to be essential for ATPase activity, and is thought to act by stabilizing the transition state of ATP hydrolysis (Ban et al., 1999; Hu et al., 1998; Meyer et al., 2003; Smith and Maxwell, 1998). Interestingly, crystal structures of the ATPase regions of DNA gyrase, topoVI, and MutL have shown that the switch loop resides outside the active site when no nucleotide is bound. When ATP binds, the transducer domain rotates 11°–18° with respect to the GHKL domain through a rearrangement of the switch loop to insert its basic residue into the ATP binding site (Ban et al., 1999; Corbett and Berger, 2003; Lamour et al., 2002; Wigley et al., 1991). This conformational change likely allows the transducer domain to communicate structural signals that affect the conformations and functions of downstream elements (Ban et al., 1999; Corbett and Berger, 2003; Oestergaard et al., 2004; Wigley et al., 1991).

Although they share very similar ATP-hydrolyzing machinery, the three subfamilies of GHL enzymes are involved in widely varying reactions. The type II topos catalyze the passage of one DNA duplex (the transfer, or "T" segment) through a transient break in another (the gate, or "G" segment). Type II topos are distributed throughout all domains of life, and include eukaryotic topo II, bacterial DNA gyrase and topoIV, and topoVI from archaea and plants (for review, see Corbett and Berger, 2004). Of these enzymes, topoVI is the smallest and simplest, and is thus a prime candidate for structural characterization (Bergerat et al., 1994, 1997). Previous structures of fragments encompassing the cata-

*Correspondence: jmberger@berkeley.edu

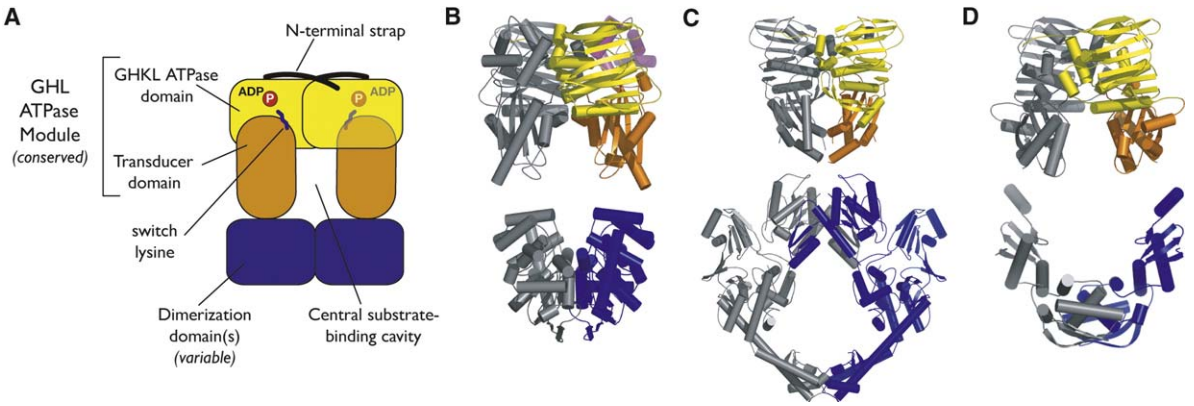

Figure 1. Structural Homology in GHKL ATPases

(A) Schematic view of GHL-family ATPases. The GHKL ATP binding domain is shown in yellow with its N-terminal strap in black, the transducer domain in orange, and diverse C-terminal dimerization domain(s) in blue. Bound ATP is represented by "ADP" and a "P" in a red circle signifies a nonhydrolyzed γ-phosphate.

(B) Predicted configuration for the topoVI holoenzyme, using separate structures of the B-subunits (ATPase module) (Corbett and Berger, 2003) and the DNA binding A subunits (Nichols et al., 1999). The regions thought to connect these subunits have not been structurally determined. Domain coloring is as in (A), except for a nonconserved, topoVI-specific "H2TH" domain (purple). One chain of the dimer is shown entirely in gray for clarity.

(C) Eukaryotic (*S. cerevisiae*) topoII built from separate structures of the ATPase module (Classen et al., 2003) and the DNA binding/cleavage region (Berger et al., 1996).

(D) MutL, built from separate structures of the ATPase module (Ban et al., 1999) and the C-terminal dimerization domain (Guarne et al., 2004). Hsp90 (not shown) is dimeric and displays a similar global architecture to these proteins (Harris et al., 2004; Meyer et al., 2003; Prodromou et al., 1997b, 2000), but its structural states are less well understood.

lytic domains of the topoVI A and B subunits have produced a rough structural model of the holoenzyme in which a dimer of ATPase (B) subunits sits atop a dimer of DNA binding and cleavage (A) subunits (Figure 1B). This organization forms a two-fold symmetric heterotetramer with two protein gates for trapping and expelling a T segment (Corbett and Berger, 2003; Nichols et al., 1999).

The role of ATP binding in triggering GHKL domain dimerization is well understood in type II topos. In contrast, the consequences of ATP hydrolysis are much more enigmatic. A nonhydrolyzable ATP analog, AMP-PNP, can be used to catalyze one round of strand passage before locking the enzyme in an unproductive state, indicating that hydrolysis is not strictly required for strand passage (Osheroff et al., 1983; Roca and Wang, 1992; Sugino et al., 1978). However, the kinetics of AMP-PNP-catalyzed strand passage are slower than the ATP-catalyzed reaction (Baird et al., 1999). In addition, although type II topos are two-fold symmetric, only one ATP is hydrolyzed prior to strand passage, whereas hydrolysis of the other does not occur until after the reaction has completed (Baird et al., 1999). Interestingly, phosphate release, as opposed to hydrolysis of the first ATP, appears to be the rate-limiting step in the reaction (Baird et al., 2001). Together, these data have raised several interesting questions about the physical role of ATP turnover in type II topos. For example, only ATP binding is required to catalyze a single turnover event, indicating that hydrolysis is not strictly needed to power a conformational change in the enzyme. However, the observation that ATP hydrolysis accelerates the reaction suggests that hydrolysis does help determine the timing and sequence of the complex motions required to effect strand passage. Another important question revolves around understanding why phosphate release is rate-limiting, as opposed to ATP hydrolysis.

We have previously reported apo and AMP-PNP bound structures of a truncated form of the *Sulfolobus shibatae* topoVI B subunit (residues 2–470, hereafter referred to as topoVI-B′) (Corbett and Berger, 2003). As with other GHL proteins, topoVI-B′ is monomeric when not bound to nucleotide and forms a dimer upon binding AMP-PNP. In this study, we have expanded on these findings by determining structures of topoVI-B′ complexed with ADP·AlF_4^-, ADP·P_i, and ADP. This study provides the most complete structural analysis to date of the ATP hydrolysis cycle of a GHL enzyme. Our data fully delineate the chemical mechanism of ATP hydrolysis, and indicate that this event regulates, but does not directly power, structural changes in the GHL ATPase module. These findings also implicate the T segment as a regulatory determinant of its own transport, and suggest that the coupling of substrate binding to ATP turnover may be a shared property in all GHL enzymes.

Results

To study the structural effects of ATP turnover in topoVI-B′, we purified and crystallized the protein in the presence of a variety of nucleotides (ATP, AMP-PNP, AMP-PCP, ATP-γ-S, ADP) and γ-phosphate/transition state analogs (aluminum and beryllium fluoride, orthovanadate, and phosphate/sulfate ions). We identified a new

crystal form for the topoVI-B′ dimer and collected more than 30 independent data sets with different substrates and crystallization conditions. We solved each structure by molecular replacement to between 2.0 and 2.2 Å resolution, and inspected the active site of each GHKL domain for unambiguous difference density that would indicate the presence of a particular nucleotide/analog. Here we present a subset of those structures that, together, make up a series of snapshots detailing each step in the ATP hydrolysis cycle of topoVI-B′. All structures were refined to working R factors of 19.5% or better, free R factors of 23.2% or better, and show good geometry, with more than 90% of residues in the most favored regions of Ramachandran space and no residues in disallowed regions (see Table S1 in the Supplemental Data available with this article online).

TopoVI-B′ Hydrolysis State

During ATP hydrolysis, the γ-phosphate passes through a trigonal planar conformation with three equatorial oxygen atoms and two axial ligands: an oxygen from the β-phosphate and the attacking water molecule. To mimic this state, we solved the structure of topoVI-B′ bound to Mg^{2+}·ADP and AlF_4^-. The AlF_4^- ion is square planar, with a central aluminum atom and four equatorial fluorine atoms possessing a formal charge of –1, and has been used extensively as a structural analog of the ATP hydrolysis transition state (Wittinghofer, 1997). In order to crystallize the topoVI-B′ Mg^{2+}·ADP·AlF_4^- complex, it was necessary to heat the protein to 65°C with free ATP and the transition state analog, and then cool it slowly to room temperature before setting crystal trays. Because *S. shibatae* is a thermophilic organism with an optimum growth temperature of ~70°C (Grogan et al., 1990), it is likely that heating allowed the protein to become more conformationally flexible, opening the active site and allowing AlF_4^- to bind.

TopoVI-B′ bound to Mg^{2+}·ADP·AlF_4^- crystallized in space group $P3_212$ with one dimer per asymmetric unit (Table S1). The structure was solved to 2.0 Å resolution by molecular replacement using as a search model the protein portion of the topoVI-B′ AMP-PNP bound dimer structure, and was refined to an R factor of 17.9% and a free R factor of 20.8%. Because the ionic state of aluminum fluoride in solution varies between AlF_3 and AlF_4^-, we screened multiple data sets until we found a condition that yielded unambiguous electron density for only one of these species plus ADP in unrefined F_o-F_c, refined $2F_o$-F_c, and simulated-annealing omit maps (Figure 2B). Because we supplied the enzyme with ATP and yet clearly observed ADP in the active site, we assume that topoVI-B′ became trapped in the ADP·AlF_4^- state after ATP hydrolysis and release of the γ-phosphate.

In the structure of topoVI-B′ bound to Mg^{2+}·ADP·AlF_4^-, the nucleotide is bound in the active site in the same conformation as was previously observed with AMP-PNP, in which one oxygen from each phosphate and the side chain of Asn42 together coordinate a single Mg^{2+} ion. The AlF_4^- moiety is held in place by hydrogen bonds between its equatorial fluorines and several backbone nitrogen atoms of the ATP lid (residues 107–111) as well as by a single fluorine-Mg^{2+} contact. The central aluminum atom of AlF_4^- also makes two axial contacts: the bridging oxygen of the ADP β-phosphate lies 2.0 Å away on one side, and a water molecule lies 2.0 Å away on the opposite side. This water molecule likely represents the nucleophilic water that initiates the hydrolysis reaction. Glu38, which is conserved in the GHL proteins and has been proposed to act as a general base during hydrolysis (Ban and Yang, 1998; Gardiner et al., 1998; Jackson and Maxwell, 1993; Obermann et al., 1998; Panaretou et al., 1998), helps position the attacking water molecule in line with the β-phosphate-aluminum vector. Gln34, in turn, hydrogen bonds Glu38 and likely helps position and polarize this residue to act as a general base. The residue equivalent to Gln34 in other type IIA topos is a histidine, but its mutation in DNA gyrase to glutamine maintains robust enzyme activity, whereas mutation to alanine abolishes ATP hydrolysis (Blance et al., 2000; Jackson and Maxwell, 1993). Lys427 from the transducer domain is positioned directly between two equatorial fluorines of AlF_4^-, consistent with its proposed role in stabilizing the developing negative charge on the γ-phosphate as hydrolysis proceeds (Corbett and Berger, 2003; Smith and Maxwell, 1998; Wigley et al., 1991).

Despite being crystallized in a new space group, the overall structure of topoVI-B′ bound to Mg^{2+}·ADP·AlF_4^-, especially the relative positions of the GHKL and transducer domains, is the same as in the previously-solved Mg^{2+}·AMP-PNP bound structure (rmsd = 0.40 Å over 461 Cα atoms) (Figure 3A). We will refer to the protein conformation observed in our dimer structures as an "ATP-restrained" state, in which the transducer domain packs tightly against the GHKL domain and is held by the contact between Lys427 and the nucleotide. This contrasts with the more "relaxed" state observed previously in the nucleotide-free monomer crystal structure, in which the switch loop and transducer domain are disengaged from the active site (Corbett and Berger, 2003) (Figures 3A and 3B).

TopoVI-B′ Product State

To characterize steps immediately following ATP hydrolysis, we next solved a 2.0 Å structure of topoVI-B′ bound to Mg^{2+}·ADP and inorganic phosphate (P_i) (R factor, 19.4%, free R factor, 23.2%). In this state, topoVI-B′ again adopts a restrained dimer configuration (overall Cα rmsd between the Mg^{2+}·AMP-PNP and Mg^{2+}·ADP·P_i dimer complexes = 0.46 Å) (Figures 2C and 3A). The additional negative charge on Mg^{2+}·ADP·P_i compared to ATP is readily accommodated by the active site. The HPO_4^{2-} ion (which is the dominant species in solution at the crystallization pH of ~8.0, and also the species likely produced by ATP hydrolysis) is oriented such that one oxygen lies within hydrogen bonding distance of Glu38; this oxygen occupies the same space as the attacking water observed in the Mg^{2+}·ADP·AlF_4^- complex. A second phosphate oxygen atom is coordinated by Lys427. Together with the transition state complex, the product bound complex indicates that ATP hydrolysis does not directly mediate any allosteric rearrangements in the enzyme.

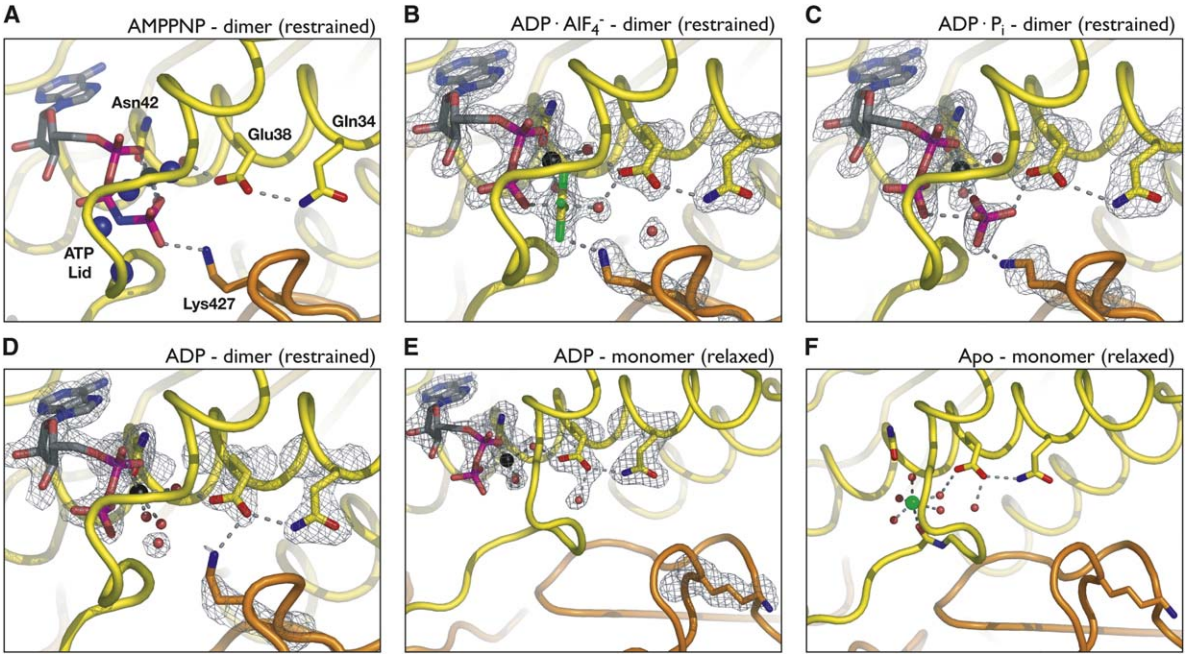

Figure 2. TopoVI-B′ Active Site Conformation in Different Nucleotide Bound States

Structures of the topoVI-B′ active site, illustrating the positions of important active site elements in six different states in the ATP hydrolysis cycle of the enzyme: (A) AMP-PNP bound dimer (Corbett and Berger, 2003); (B) ADP·AlF_4^- bound dimer; (C) ADP·P_i bound dimer; (D) ADP bound dimer; (E) ADP bound monomer; and (F) Apo monomer (Corbett and Berger, 2003). The GHKL domain is shown in yellow, the transducer domain in orange, main-chain nitrogen atoms of residues 107–111 (A only) in blue, Mg^{2+} ions in black, and the Ca^{2+} ion in the apo structure in green. For the four structures reported here (B–E), density from simulated annealing omit F_o-F_c maps is shown contoured at 3.0 σ (maps were calculated omitting the noted active site residues, nucleotide, and coordinating water molecules). The Mg^{2+} ion and coordinating waters in the ADP bound dimer structure (D) have high B factors (~50 $Å^2$) and, thus, the simulated annealing density is below the displayed contour level (1.5–2.0 σ).

TopoVI-B′ Product Release States

In the restrained dimer state, the active site of topoVI-B′ and other GHL ATPases completely sequesters a bound nucleotide from solvent (Ban et al., 1999; Corbett and Berger, 2003; Wigley et al., 1991). As a result, free P_i is trapped within the active site after hydrolysis, and is thought to require a conformational change for release. Previous kinetic experiments with *Saccharomyces cerevisiae* topoII have pointed to P_i release as a key point in the mechanism of type II topos, coincident with the rate-limiting step of strand passage (Baird et al., 2001). Because of the evident importance of this step, we sought to better understand the process of P_i release by topoVI-B′. To accomplish this, we solved a 2.2 Å structure of topoVI-B′ bound to Mg^{2+}·ADP (R factor, 19.5%, free R factor, 23.1%). In this structure, the protein is in a dimeric state with a global architecture and active site structure almost exactly equivalent to our other nucleotide bound complexes (overall Cα rmsd between the Mg^{2+}·AMP-PNP and Mg^{2+}·ADP dimer complexes = 0.45 Å) (Figures 2D and 3A). The only significant difference we observe is that Glu38 and Lys427 hydrogen bond to each other in the absence of a γ-phosphate. Thus, even without a γ-phosphate to position Lys427 and the switch loop, the closed active site and the restrained GHKL/transducer domain arrangement can be preserved in the ADP bound state. The conformation of the ATP lid is also maintained in the absence of a γ-phosphate, due to interactions with the transducer domain and the N-terminal strap of the dimer mate (see Figure S1).

Given that the topoVI-B′ active site is sequestered from solvent in structures mimicking both the pre- and post-P_i release states, a question arises as to the nature of conformational changes that could allow P_i release. To address this question, we studied a second crystal morphology similar to that of our previous topoVI-B′ apo crystals (Corbett and Berger, 2003) that grew readily in the presence of Mg^{2+}·ADP, and solved the structure to 2.1 Å resolution (R factor, 18.9%, free R factor, 22.8%). TopoVI-B′ in this crystal form was monomeric, yet still bound to Mg^{2+}·ADP (Figure 2E). Although the base and sugar moieties of ADP are coordinated normally by the protein, the active site in this state does not appear competent for hydrolysis: the γ-phosphate binding elements of the active site, including the ATP lid and the switch loop containing Lys427, have moved significantly away from the positions seen in other nucleotide bound structures. As a result of this motion, the GHKL and transducer domains relax away from each other, adopting a relative orientation similar to that of the previously solved apo monomer structure (overall Cα rmsd between the apo and Mg^{2+}·ADP bound monomer structures = 0.49 Å) (Figure 3A). This structure shows how the active site is altered after separation of the GHKL domain dimer, indicating how ADP

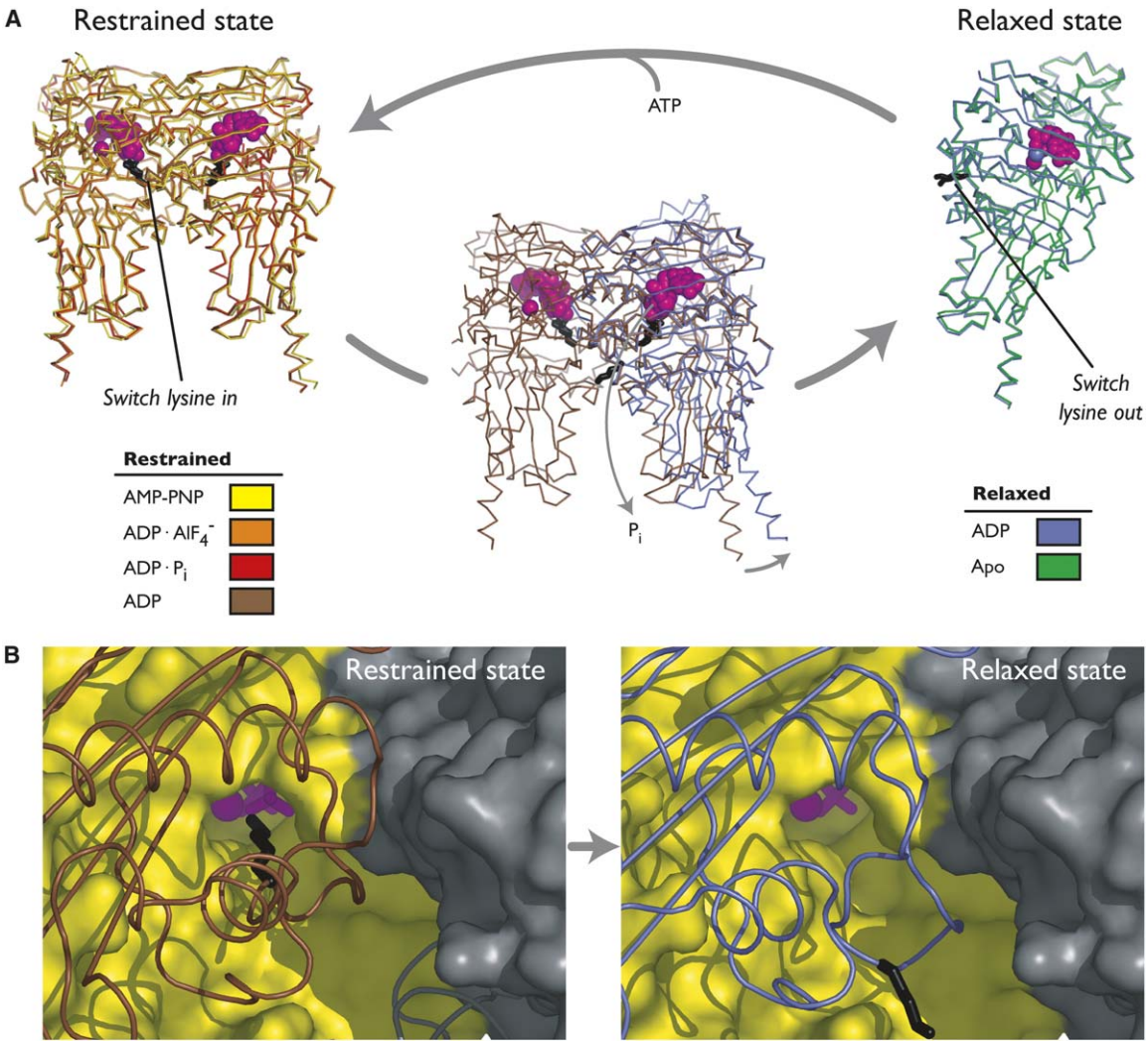

Figure 3. TopoVI-B′ Subunit Conformation in Different Nucleotide Bound States

(A) Overlays of multiple topoVI-B′ structures in different nucleotide bound and oligomeric states, arranged in an outline of the ATP hydrolysis cycle. The two ADP bound states are shown overlaid in the center, highlighting the structural transition from the restrained to the relaxed state. AMP-PNP bound topoVI-B′ (Corbett and Berger, 2003) is shown in yellow, ADP·AlF_4^- in orange, ADP·P_i in red, ADP (dimer state) in brown, ADP (monomer state) in blue, and Apo (Corbett and Berger, 2003) in green. Lys427 ("switch lysine") is shown in black, with nucleotides and Mg^{2+} ions in magenta. The Ca^{2+} ion bound in the active site of the apo form is shown in light blue.

(B) Bottom views of the restrained and relaxed states, showing the tunnel into which Lys427 is inserted in the restrained state and through which P_i is released in the relaxed state. The GHKL domain is shown as a yellow surface with the dimer-related chain in gray; the transducer domain is shown as a brown (restrained state) or blue (relaxed state) coil.

is released to reset the enzyme. Because the protein conformation we observed in these crystals is limited by crystal packing interactions, this structure likely represents only one of a range of conformations available to the subunit after uncoupling of the GHKL and transducer domains.

To confirm that both ADP bound structures represent relevant functional states of topoVI, we assayed dimerization of topoVI-B′ in solution using glutaraldehyde cross-linking assays. These experiments show that ADP, ATP, and AMP-PNP all stimulate dimerization to a similar extent (Figure S2), supporting the notion that ADP can promote/stabilize the GHKL domain dimer. Interestingly, ADP has also been shown to stabilize a closed GHKL domain dimer in both human and *S. cerevisiae* topoII (Hu et al., 2002; Vaughn et al., 2005). This is in contrast to the related GHL ATPases, MutL and Hsp90, in which ADP is unable to stabilize dimers of the isolated ATPase regions in solution but does stabilize a crystallographic dimer of MutL (Ban and Yang, 1998; Ban et al., 1999; Prodromou et al., 2000).

Extensive attempts to crystallize topoVI-B′ in the relaxed, monomeric form bound to any nucleotide bearing a γ-phosphate analog (e.g., ATP or AMP-PNP) were unsuccessful, suggesting that ADP is the only nucleotide compatible with the relaxed conformation adopted in the monomer crystals. Together, these observations are consistent with the idea that the transition from a

restrained to a relaxed state cannot occur until after ATP hydrolysis. The two ADP bound structures thus appear to reflect two reaction states: one in which ATP has been hydrolyzed and P_i released (post T segment transport), and another in which the ATPase domains have reopened but not yet released ADP (pre-enzyme resetting). The structures also provide a means for understanding how P_i can diffuse out of the active site: following ATP hydrolysis, the transducer domain may transiently uncouple from the GHKL domain and move into a relaxed state, opening the active site to solvent through a tunnel vacated by the switch loop and Lys427 (Figure 3).

The conformational change observed between the restrained and relaxed conformations is a rotation of approximately 11° between the GHKL and transducer domains. This event is initiated by rotation of the switch loop, and is amplified through the transducer domain to move the C-terminal α helix by 15 Å. Detailed analysis of the two states of topoVI-B′ has allowed us to identify two residues in this protein, Gln103 in the GHKL domain, and Asn375 in the transducer domain, that link the two domains together by hydrogen bonds in both the monomer and dimer states, and appear to act as a pivot point for the interdomain rotation. Sequence analysis of other GHKL enzymes show that Gln103 is not well conserved outside of topoVI, but that Asn375 is highly conserved throughout type II topos. Crystal structures of the ATPase regions of *Escherichia coli* GyrB and *S. cerevisiae* topoII indicate that, as in topoVI-B′, this residue links the GHKL and transducer domains through hydrogen bonds (Classen et al., 2003; Lamour et al., 2002; Wigley et al., 1991). Curiously, this asparagine is also conserved in MutL proteins, even though it makes no hydrogen bonds with the GHKL domain and the restrained-to-relaxed transition in MutL does not hinge around this residue (Ban and Yang, 1998; Ban et al., 1999). The asparagine is not conserved in Hsp90. In this enzyme, however, the GHKL and transducer domains are attached to one another by a long (20–30 amino acid) linker, and it has been suggested that the nucleotide-dependent structural switch in Hsp90 proteins may result from the association and dissociation of the two domains, instead of an interdomain rotation, as seen in type II topos and MutL (Meyer et al., 2003).

Discussion

Mechanism and Conformational Effects of ATP Hydrolysis

Together with the previously solved apo and AMP-PNP bound forms (Corbett and Berger, 2003), our structures of topoVI-B′ bound to ADP·AlF_4^-, ADP·P_i, and ADP provide a detailed outline of the nucleotide hydrolysis cycle of type II topos (Figure 4). Previously proposed roles for several active-site residues conserved in the GHL family are confirmed by these structures. Glu38 (numbering according to topoVI-B′), positioned by Gln34, polarizes a water molecule for in-line attack on the γ-phosphate of ATP. Hydrolysis then proceeds with the developing negative charge of the planar transition state stabilized by Lys427 and by the main-chain nitrogen atoms of the ATP lid (residues 107–111). Following hydrolysis, P_i is coordinated by Lys427 and Glu38 until its release from the active site.

Our data show that, as in type IIA topos and MutL, ATP binding to topoVI-B′ causes two protomers to dimerize and reorients the transducer domain into an "ATP-restrained" state (Corbett and Berger, 2003). These conformational changes sequester ATP from solution and organize the active site for hydrolysis. Remarkably, topoVI-B′ appears to maintain this restrained conformation throughout ATP hydrolysis (Figure 2). This finding is significant, because for ADP and P_i to be released, the active site must be reorganized and opened to solvent. Clues to this event arise from our two structures of ADP-bound topoVI-B′. In one, the protein adopts a dimeric, restrained state that is essentially identical to other nucleotide bound structures. In the other, the protein adopts a monomeric, relaxed conformation in which the transducer domain has rotated away from the GHKL domain, opening the active site for product release. Taken together with our dimerization assays, these data indicate that the interdomain motions between the GHKL and transducer domains are restricted until the covalent β-γ phosphate linkage is broken, and that ATP hydrolysis does not directly drive any changes in subunit conformation. Instead, hydrolysis appears to be a prerequisite for a conformational change, which is then presumably powered by another source.

Role of ATP Turnover in Strand Passage by Type II Topos

The above model is congruent with many biochemical properties of type II topos. For example, experiments using nonhydrolyzable ATP analogs have shown that hydrolysis is not required for a single strand passage event (Roca and Wang, 1992; Sugino et al., 1978; Osheroff et al., 1983). Nonetheless, kinetic experiments with *S. cerevisiae* topoII have established that one ATP is hydrolyzed before the passage of the T segment through the G segment (Baird et al., 1999). This hydrolysis event accelerates strand passage over the rate seen with nonhydrolyzable analogs (Baird et al., 1999), but curiously is not the rate-limiting step in the reaction. Instead, P_i release from the ATPase module represents the slow step of strand passage (Baird et al., 2001). These results have implied that a conformational change in the protein is necessary to release P_i, and that this motion is coupled to strand passage (Baird et al., 2001).

The structural data we have obtained with topoVI-B′ are consistent with such a mechanism (Figure 5). Our results indicate not only that ATP hydrolysis does not directly mediate a conformational change in the ATPase subunit of type II topos, but also that a significant conformational change must occur to release P_i from the active site. The γ-phosphate moiety is likely to be a key player in coordinating this event, initially locking the transducer domain into a restrained state through its interaction with Lys427, but permitting the transition to a relaxed state after hydrolysis. Because the transducer domain is tethered to the G segment binding region of the enzyme, the transducer domain likely propagates

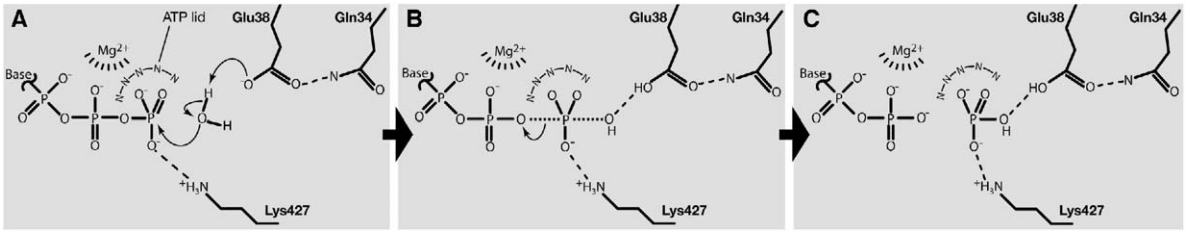

Figure 4. Proposed Mechanism of ATP Hydrolysis by TopoVI-B′

(A) Gln34 helps position Glu38 in the active site, which acts as a general base to abstract a proton from the attacking water molecule.

(B) The γ-phosphate passes through a pentavalent transition state, in which negative charge on the nonbridging oxygens is stabilized by Lys427, Mg^{2+}, and main-chain nitrogen atoms of the ATP lid (amino acids 107–111). The reaction has been modeled as mostly dissociative in nature, although the presence of positively charged groups surrounding the γ-phosphate suggests the possibility of at least partial associative character (Maegley et al., 1996; O'Brien and Herschlag, 1999).

(C) Completion of hydrolysis results in ADP·P_i bound in the active site. The view for all three panels is equivalent to the view in Figure 2, with states in (A), (B), and (C) corresponding to Figures 2A, 2B, and 2C, respectively.

its conformational changes into this region, consistent with the observation that P_i release is concomitant with strand passage.

If ATP hydrolysis does not drive conformational changes between the GHKL and transducer domains, what else might cause this motion? One candidate for the power source is the trapped T segment itself. Multiple structures of the ATPase regions from several type II topos have shown that the space between the two protomers might be too small to comfortably accommodate a duplex DNA (Bellon et al., 2004; Classen et al., 2003; Corbett and Berger, 2003; Lamour et al., 2002; Wigley et al., 1991). However, there is evidence that the T segment can interact with the inner surface of the transducer domain, as well as affect G segment cleavage (Corbett et al., 1992; Tingey and Maxwell, 1996). T segment binding could lead to strain within a dimerized ATPase module, pushing outwards on the transducer domains when they are in the ATP-restrained state (Figure 5). If this is the case, then ATP hydrolysis might serve to loosen the connection between the GHKL and transducer domains, and allow the T segment to drive conformational changes to complete strand passage.

A role for strain induced by the T segment in deter-

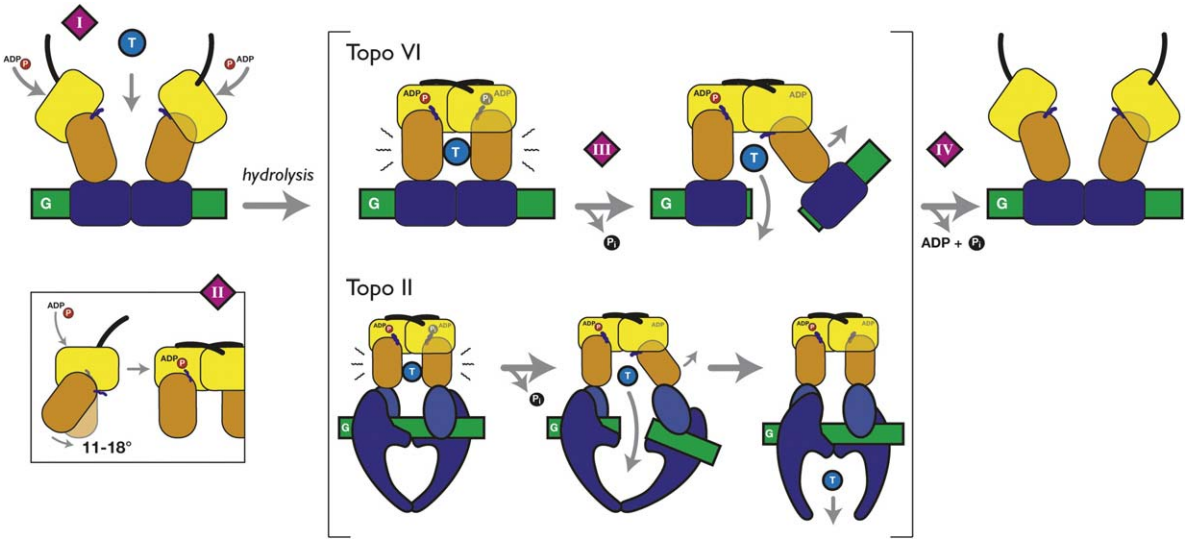

Figure 5. Model for ATP Hydrolysis and Strand Passage in Type II Topos

Schematic view of the reactions of topoVI (top) and topoII (bottom). The enzyme first binds a G segment (green), then binds two ATP molecules and a T segment (blue), and dimerization of the GHKL domains traps the T segment inside the enzyme (I). ATP binding, in addition to mediating dimerization, causes reorientation of the transducer and GHKL domains into an "ATP-restrained" state (II). GHKL dimerization around a T segment and the conformation change to the restrained state combine to create strain on the transducer domains, represented here by zig-zag lines. Some time after hydrolysis of one ATP, the strain applied by the T segment is able to cause a structural transition in the ATPase module that, in turn, forces apart the A subunit dimer and the cleaved G segment to complete strand passage (III). Reclosing of the A subunit and hydrolysis of the second ATP allows enzyme resetting (IV). Domains are colored as in Figure 1. A nonhydrolyzed γ-phosphate is represented by "P" in a red circle, and a hydrolyzed γ-phosphate is represented by "P_i" in a black circle. The asymmetric nature of ATP hydrolysis by topoII has been well established; given the structural similarity of topoVI, we anticipate that this enzyme will behave likewise.

mining the structural state of the ATPase module can explain why some type II topos, when supplied with a nonhydrolyzable ATP analog (AMP-PNP), can nevertheless catalyze one or more rounds of duplex DNA passage (Osheroff et al., 1983; Sugino et al., 1980; Williams et al., 2001). In these instances, the conformational change from an ATP-restrained to a relaxed state would not be strictly dependent on ATP hydrolysis to loosen the GHKL-transducer connection. Over time, strain applied by the T segment could force the γ-phosphate/switch lysine interaction to break, allowing T segment passage and release. Once the T segment is expelled, the restrained state could then reform around AMP-PNP, thereby preventing enzyme resetting. Overall, these concepts cast the transducer domain in a potentially new and important mechanistic role, both as a sensor for the productive association of a DNA substrate and as a mediator that links this binding event with the hydrolysis of ATP to regulate the subsequent steps of strand passage in type II topos.

Implications for Other GHL ATPases

Some aspects of these findings may also be applicable to other GHL enzymes. The machinery utilized for ATP binding and hydrolysis is well conserved between MutL, Hsp90, and type II topos. It is therefore possible that the mechanism and structural effects of ATP hydrolysis and product release we observe for topoVI-B′ are maintained to some extent in these protein families as well.

MutL is part of a conserved mismatch repair system that includes the MutS protein and a number of downstream effectors. After MutS recognizes and binds a mismatched base pair, it associates with MutL, triggering a cascade of events that leads to lesion repair (Schofield and Hsieh, 2003). In bacteria, MutL interacts with the MutH endonuclease (Hall and Matson, 1999) and the UvrD helicase (Guarne et al., 2004). Binding to both MutH and UvrD is dependent on ATP binding by MutL, and directly involves surfaces on the ATPase module (Ban and Yang, 1998; Giron-Monzon et al., 2004; Guarne et al., 2004). Additionally, MutL binds both double and single-stranded DNA, probably inside the cavity formed by the two dimer interfaces, and DNA binding stimulates ATP hydrolysis by the enzyme (Ban et al., 1999; Guarne et al., 2004). These properties hint at a possible parallel with the mechanisms of type II topos, whereby the transducer domains of MutL could sense and respond to DNA binding, thereby modulating the nucleotide state and the GHKL/transducer domain juxtaposition of the protein, and potentially affecting its interactions with downstream functional partners.

Several structures of MutL bound to various nucleotides show compelling mechanistic parallels between this enzyme and the type II topos. MutL adopts a closed dimer state when bound to either AMP-PNP or ADP (Ban et al., 1999), supporting the notion that there exists a preferred nucleotide bound "restrained" state in the dimeric forms of GHL enzymes. The apo form of MutL is monomeric with a more open domain juxtaposition, again closely paralleling the "relaxed" state of topoVI-B′ (Ban and Yang, 1998).

ATP hydrolysis is likely also utilized as a switch in Hsp90 chaperones. Several studies have suggested that Hsp90 client proteins bind inside the cavity created by two dimer-related ATPase modules. Residues involved in these interactions reside both on the transducer domain (Meyer et al., 2003, 2004; Sato et al., 2000) and on the C-terminal dimerization domain (Harris et al., 2004; Yamada et al., 2003). The GHKL and transducer domains in Hsp90 are separated by a stretch of disordered residues (Meyer et al., 2003), which may mean that the two domains can alternately engage and disengage each other in response to nucleotide state. It is intriguing to consider whether the transducer domains might play an active role in sensing the state of a bound client protein to modulate ATP hydrolysis in these enzymes.

Conclusions

In summary, this work represents a complete structural map for the nucleotide hydrolysis mechanism of topoVI. Our data show that ATP turnover does not directly power structural changes within the enzyme, but rather controls the timing and order of conformational events that lead to DNA cleavage and strand passage by acting as a prerequisite for a structural rearrangement. In addition, the T segment may play a direct role in regulating or powering this motion. This work helps define the GHKL and transducer domains as an ATPase module capable of providing a ligand-responsive structural switch in type II topos, a concept that may prove useful when considering the role of substrate binding and ATP turnover in the related MutL and Hsp90 proteins.

Experimental Procedures

Crystallization

A construct containing residues 2–470 of the *S. shibatae* topoVI B-subunit (topoVI-B′) was cloned and purified as described previously (Corbett and Berger, 2003). For crystallization trials, purified topoVI-B′ at 10–15 mg/mL was dialyzed overnight against 20 mM Tris-HCl (pH 7.0), 0.1 M NaCl, and the protein concentration was adjusted to 10–12 mg/mL. For some crystallization trials, selenomethionine-substituted topoVI-B′ was used (Van Duyne et al., 1993). In these trials, 0.5 mM Tris(2-carboxyethyl)phosphine (TCEP) (Fluka) was included in the dialysis buffer as a reducing agent.

For the topoVI-B′ Mg^{2+}·ADP·AlF_4^- complex, crystallization was performed in hanging drop format. To dialyzed topoVI-B′, ATP was added to 1 mM, $MgCl_2$ to 5 mM, $AlCl_3$ to 5 mM, and NaF to 25 mM. The protein solution was incubated at 65°C for 90 min, then slowly cooled to 20°C, whereupon crystallization trays were set by mixing the protein solution in a 1:1 ratio with well solution containing 0.1 M Tris-HCl (pH 8.0), 0.1 M $LiSO_4$, 13% PEG-4000, and 29% glycerol. Crystals (hexagonal plates ~0.3 × 0.3 × 0.1 mm) grew within 1 week, were looped directly from the drop, and were flash-frozen in liquid nitrogen. The crystals (as well as those of the other topoVI-B′ dimer crystals) belong to space group $P3_212$ and contain one dimer in the asymmetric unit (Table S1).

For the topoVI-B′ Mg^{2+}·ADP·P_i complex, crystallization was performed in hanging drop format. Dialyzed selenomethionine-labeled topoVI-B′ was mixed 1:1 with well solution containing 0.1 M K_2HPO_4, 10% PEG-3350, 10% 2-methyl-1,3 propanediol (MPD), 1 mM ADP, 5 mM $MgCl_2$, 25 mM NaF, and 0.5 mM TCEP at 20°C. Crystals were transferred to cryoprotectant solution containing an additional 15% MPD (25% MPD total) for 1 minute, then looped from the drop, and flash-frozen in liquid nitrogen. These crystallization conditions were originally intended to produce a topoVI-B′ Mg^{2+} ADP·MgF_3 planar transition-state analog complex, but difference density clearly showed the presence of the HPO_4^{2-} ion.

For the topoVI-B′ Mg^{2+}·ADP dimer complex, crystallization was

performed in hanging drop format. Dialyzed topoVI-B′ was mixed 1:1 with well solution containing 0.1 M Tris-HCl (pH 8.5), 0.1 M $LiSO_4$, 14% PEG-4000, 1 mM ADP, 5 mM $MgCl_2$, and 30% glycerol at 20°C. Crystals were looped directly from the drop and flash-frozen in liquid nitrogen. The final pH of crystallization conditions for all dimer complexes was between 8.0 and 8.5.

For the topoVI-B′ Mg^{2+}·ADP monomer complex, crystallization was performed in microbatch format under paraffin oil. Selenomethionine-labeled topoVI-B′ was dialyzed into 20 mM HEPES (pH 7.5), 0.1 M NaCl, 5 mM $MgCl_2$, and 0.1 mM ADP, and then 1 mM ADP was added to the protein solution. This was mixed 1:1 with well solution containing 0.2 M $Mg(HCO_2)_2$ and 20% PEG-3350 at 20°C. The crystallization drop was flooded with cryoprotectant containing an additional 25% glycerol, then crystals (flat plates ~0.2 × 0.2 × 0.02 mm) were flash-frozen in liquid nitrogen.

Data Collection and Structure Solution

All data sets were collected on Beamline 8.3.1 at the Advanced Light Source at Lawrence Berkeley National Laboratory (MacDowell et al., 2004). Data for all crystals were indexed and reduced with DENZO/SCALEPACK (Otwinowski and Minor, 1997). The CCP4 set of programs was used for truncating and scaling the data sets (Collaborative Computational Project, 1994). Phases were determined by molecular replacement with AMoRe (Navaza, 2001), using the previously solved topoVI-B′ apo and AMP-PNP bound structures (PDB ID 1MU5 and 1MX0, respectively) with ligands extracted as search models. Consistent free-R sets were used for all data sets within a single space group to avoid inadvertently refining against previously free reflections. Refinement and placement of ordered water molecules for all models was carried out using a Refmac/ARP procedure (Lamzin and Wilson, 1993; Murshudov et al., 1997), followed by TLS refinement as implemented in Refmac5 (Winn et al., 2001). F_o-F_c simulated annealing omit maps were generated by CNS (Brunger et al., 1997, 1998). Figures were produced with PyMOL (DeLano, 2002).

Supplemental Data

Supplemental data, including an additional table and figures, are available at http://www.structure.org/cgi/content/full/13/6/873/DC1/.

Acknowledgments

The authors thank E. Skordalakes for assistance with data collection and structure solution, J.M. Holton, G. Meigs, and J. Tanamachi for assistance at ALS Beamline 8.3.1, and D. Akey, D.S. Classen, and J. Erzberger for helpful discussions. K.D.C. acknowledges support from a National Science Foundation Graduate Research Fellowship, and J.M.B. acknowledges support from the National Institutes of Health (CA 77373).

Received: January 31, 2005
Revised: March 12, 2005
Accepted: March 21, 2005
Published: June 7, 2005

References

Baird, C.L., Gordon, M.S., Andrenyak, D.M., Marecek, J.F., and Lindsley, J.E. (2001). The ATPase reaction cycle of yeast DNA topoisomerase II: slow rates of ATP resynthesis and P_i release. J. Biol. Chem. *276*, 27893–27898.

Baird, C.L., Harkins, T.T., Morris, S.K., and Lindsley, J.E. (1999). Topoisomerase II drives DNA transport by hydrolyzing one ATP. Proc. Natl. Acad. Sci. USA *96*, 13685–13690.

Ban, C., Junop, M., and Yang, W. (1999). Transformation of MutL by ATP binding and hydrolysis: a switch in DNA mismatch repair. Cell *97*, 85–97.

Ban, C., and Yang, W. (1998). Crystal structure and ATPase activity of MutL: implications for DNA repair and mutagenesis. Cell *95*, 541–552.

Bellon, S., Parsons, J.D., Wei, Y., Hayakawa, K., Swenson, L.L., Charifson, P.S., Lippke, J.A., Aldape, R., and Gross, C.H. (2004). Crystal structures of the *Escherichia coli* topoisomerase IV ParE subunit (24 and 43 kilodaltons): a single residue dictates differences in novobiocin potency against topoisomerase IV and DNA gyrase. Antimicrob. Agents Chemother. *48*, 1856–1864.

Berger, J.M., Gamblin, S.J., Harrison, S.C., and Wang, J.C. (1996). Structure and mechanism of DNA topoisomerase II. Nature *379*, 225–232.

Bergerat, A., De Massy, B., Gadelle, D., Varoutas, P.-C., Nicolas, A., and Forterre, P. (1997). An atypical topoisomerase II from archaea with implications for meiotic recombination. Nature *386*, 414–417.

Bergerat, A., Gadelle, D., and Forterre, P. (1994). Purification of a DNA topoisomerase II from the hyperthermophilic archaeon *Sulfolobus shibatae*: a thermostable enzyme with both bacterial and eucaryal features. J. Biol. Chem. *269*, 27663–27669.

Blance, S.J., Williams, N.L., Preston, Z.A., Bishara, J., Smyth, M.S., and Maxwell, A. (2000). Temperature-sensitive suppressor mutations of the *Escherichia coli* DNA gyrase B protein. Protein Sci. *9*, 1035–1037.

Brunger, A.T., Adams, P.D., Clore, G.M., DeLano, W.L., Gros, P., Grosse-Kunstleve, R.W., Jiang, J.S., Kuszewski, J., Nilges, M., Pannu, N.S., et al. (1998). Crystallography & NMR system: a new software suite for macromolecular structure determination. Acta Crystallogr. D Biol. Crystallogr. *54*, 905–921.

Brunger, A.T., Adams, P.D., and Rice, L.M. (1997). New applications of simulated annealing in X-ray crystallography and solution NMR. Structure *5*, 325–336.

Classen, D.S., Olland, S., and Berger, J.M. (2003). Structure of the topoisomerase II ATPase region and its mechanism of inhibition by the chemotherapeutic, ICRF-187. Proc. Natl. Acad. Sci. USA *100*, 10629–10634.

Collaborative Computational Project, N. (1994). The CCP4 suite: programs for protein crystallography. Acta Crystallogr. D Biol. Crystallogr. *50*, 760–763.

Corbett, A.H., Zechiedrich, E.L., and Osheroff, N. (1992). A role for the passage helix in the DNA cleavage reaction of eukaryotic topoisomerase II: a two-site model for enzyme-mediated DNA cleavage. J. Biol. Chem. *267*, 683–686.

Corbett, K.D., and Berger, J.M. (2003). Structure of the topoisomerase VI B subunit: implications for type II topoisomerase mechanism and evolution. EMBO J. *22*, 151–163.

Corbett, K.D., and Berger, J.M. (2004). Structure, molecular mechanisms, and evolutionary relationships in DNA topoisomerases. Annu. Rev. Biophys. Biomol. Struct. *33*, 95–118.

DeLano, W.L. (2002). PyMOL (San Carlos, CA: DeLano Scientific).

Dutta, R., and Inouye, M. (2000). GHKL, an emergent ATPase/kinase superfamily. Trends Biochem. Sci. *25*, 24–28.

Gardiner, L.P., Roper, D.I., Hammonds, T.R., and Maxwell, A. (1998). The N-terminal domain of human topoisomerase IIα is a DNA-dependent ATPase. Biochemistry *37*, 16997–17004.

Giron-Monzon, L., Manelyte, L., Ahrends, R., Kirsch, D., Spengler, B., and Friedhoff, P. (2004). Mapping protein-protein interactions between MutL and MutH by cross-linking. J. Biol. Chem. *279*, 49338–49345.

Grogan, D., Palm, P., and Zillig, W. (1990). Isolate B12, which harbours a virus-like element, represents a new species of the archaebacterial genus *Sulfolobus, Sulfolobus shibatae*, sp. nov. Arch. Microbiol. *154*, 594–599.

Guarne, A., Ramon-Maiques, S., Wolff, E.M., Ghirlando, R., Hu, X., Miller, J.H., and Yang, W. (2004). Structure of the MutL C-terminal domain: a model of intact MutL and its roles in mismatch repair. EMBO J. *23*, 4134–4145.

Hall, M.C., and Matson, S.W. (1999). The *Escherichia coli* MutL protein physically interacts with MutH and stimulates the MutH-associated endonuclease activity. J. Biol. Chem. *274*, 1306–1312.

Harris, S.F., Shiau, A.K., and Agard, D.A. (2004). The crystal structure of the carboxy-terminal dimerization domain of htpG, the

Escherichia coli Hsp90, reveals a potential substrate binding site. Structure *12*, 1087–1097.

Hu, T., Chang, S., and Hsieh, T. (1998). Identifying Lys359 as a critical residue for the ATP-dependent reactions of *Drosophila* DNA topoisomerase II. J. Biol. Chem. *273*, 9586–9592.

Hu, T., Sage, H., and Hsieh, T.S. (2002). ATPase domain of eukaryotic DNA topoisomerase II: inhibition of ATPase activity by the anticancer drug bisdioxopiperazine and ATP/ADP-induced dimerization. J. Biol. Chem. *277*, 5944–5951.

Jackson, A.P., and Maxwell, A. (1993). Identifying the catalytic residue of the ATPase reaction of DNA gyrase. Proc. Natl. Acad. Sci. USA *90*, 11232–11236.

Lamour, V., Hoermann, L., Jeltsch, J.-M., Oudet, P., and Moras, D. (2002). An open conformation of the *Thermus thermophilus* gyrase B ATP-binding domain. J. Biol. Chem. *277*, 18947–18953.

Lamzin, V.S., and Wilson, K.S. (1993). Automated refinement of protein models. Acta Crystallogr. D Biol. Crystallogr. *49*, 129–147.

MacDowell, A.A., Celestre, R.S., Howells, M., McKinney, W., Krupnick, J., Cambie, D., Domning, E.E., Duarte, R.M., Kelez, N., Plate, D.W., et al. (2004). Suite of three protein crystallography beamlines with single superconducting bend magnet as the source. J. Synchrotron Radiat. *11*, 447–455.

Maegley, K.A., Admiraal, S.J., and Herschlag, D. (1996). Ras-catalyzed hydrolysis of GTP: a new perspective from model studies. Proc. Natl. Acad. Sci. USA *93*, 8160–8166.

Meyer, P., Prodromou, C., Hu, B., Vaughan, C., Roe, S.M., Panaretou, B., Piper, P.W., and Pearl, L.H. (2003). Structural and functional analysis of the middle segment of Hsp90: implications for ATP hydrolysis and client protein and cochaperone interactions. Mol. Cell *11*, 647–658.

Meyer, P., Prodromou, C., Liao, C., Hu, B., Mark Roe, S., Vaughan, C.K., Vlasic, I., Panaretou, B., Piper, P.W., and Pearl, L.H. (2004). Structural basis for recruitment of the ATPase activator Aha1 to the Hsp90 chaperone machinery. EMBO J. *23*, 511–519.

Murshudov, G.N., Vagin, A.A., and Dodson, E.J. (1997). Refinement of macromolecular structures by the maximum-likelihood method. Acta Crystallogr. D Biol. Crystallogr. *53*, 240–255.

Navaza, J. (2001). Implementation of molecular replacement in AMoRe. Acta Crystallogr. D Biol. Crystallogr. *57*, 1367–1372.

Nichols, M.D., DeAngelis, K., Keck, J.L., and Berger, J.M. (1999). Structure and function of an archaeal topoisomerase VI subunit with homology to the meiotic recombination factor Spo11. EMBO J. *18*, 6177–6188.

O'Brien, P.J., and Herschlag, D. (1999). Does the active site arginine change the nature of the transition state for alkaline phosphatase-catalyzed phosphoryl transfer? J. Am. Chem. Soc. *121*, 11022–11023.

Obermann, W.M., Sondermann, H., Russo, A.A., Pavletich, N.P., and Hartl, F.U. (1998). *In vivo* function of Hsp90 is dependent on ATP binding and ATP hydrolysis. J. Cell Biol. *143*, 901–910.

Oestergaard, V.H., Bjergbaek, L., Skouboe, C., Giangiacomo, L., Knudsen, B.R., and Andersen, A.H. (2004). The transducer domain is important for clamp operation in human DNA topoisomerase IIα. J. Biol. Chem. *279*, 1684–1691.

Osheroff, N., Shelton, E.R., and Brutlag, D.L. (1983). DNA topoisomerase II from *Drosophila melanogaster*: relaxation of supercoiled DNA. J. Biol. Chem. *258*, 9536–9543.

Otwinowski, Z., and Minor, W. (1997). Processing of X-ray diffraction data collected in oscillation mode. Methods Enzymol. *276*, 472–494.

Panaretou, B., Prodromou, C., Roe, S.M., O'Brien, R., Ladbury, J.E., Piper, P.W., and Pearl, L.H. (1998). ATP binding and hydrolysis are essential to the function of the Hsp90 molecular chaperone in vivo. EMBO J. *17*, 4829–4836.

Prodromou, C., Panaretou, B., Chohan, S., Siligardi, G., O'Brien, R., Ladbury, J.E., Roe, S.M., Piper, P.W., and Pearl, L.H. (2000). The ATPase cycle of Hsp90 drives a molecular "clamp" via transient dimerization of the N-terminal domains. EMBO J. *19*, 4383–4392.

Prodromou, C., Roe, S.M., O'Brien, R., Ladbury, J.E., Piper, P.W., and Pearl, L.H. (1997a). Identification and structural characterization of the ATP/ADP-binding site in the Hsp90 molecular chaperone. Cell *90*, 65–75.

Prodromou, C., Roe, S.M., Piper, P.W., and Pearl, L.H. (1997b). A molecular clamp in the crystal structure of the N-terminal domain of the yeast Hsp90 chaperone. Nat. Struct. Biol. *4*, 477–482.

Roca, J., and Wang, J.C. (1992). The capture of a DNA double helix by an ATP-dependent protein clamp: a key step in DNA transport by type II DNA topoisomerases. Cell *71*, 833–840.

Sato, S., Fujita, N., and Tsuruo, T. (2000). Modulation of Akt kinase activity by binding to Hsp90. Proc. Natl. Acad. Sci. USA *97*, 10832–10837.

Schofield, M.J., and Hsieh, P. (2003). DNA mismatch repair: molecular mechanisms and biological function. Annu. Rev. Microbiol. *57*, 579–608.

Smith, C.V., and Maxwell, A. (1998). Identification of a residue involved in transition-state stabilization in the ATPase reaction of DNA gyrase. Biochemistry *37*, 9658–9667.

Sugino, A., Higgins, N.P., Brown, P.O., Peebles, C.L., and Cozzarelli, N.R. (1978). Energy coupling in DNA gyrase and the mechanism of action of novobiocin. Proc. Natl. Acad. Sci. USA *75*, 4838–4842.

Sugino, A., Higgins, N.P., and Cozzarelli, N.R. (1980). DNA gyrase subunit stoichiometry and the covalent attachment of subunit A to DNA during DNA cleavage. Nucleic Acids Res. *8*, 3865–3874.

Tingey, A.P., and Maxwell, A. (1996). Probing the role of the ATP-operated clamp in the strand-passage reaction of DNA gyrase. Nucleic Acids Res. *24*, 4868–4873.

Van Duyne, G.D., Standaert, R.F., Karplus, P.A., Schreiber, S.L., and Clardy, J. (1993). Atomic structures of the human immunophilin FKBP-12 complexes with FK506 and rapamycin. J. Mol. Biol. *229*, 105–124.

Vaughn, J., Huang, S., Wessel, I., Sorensen, T.K., Hsieh, T., Jensen, L.H., Jensen, P.B., Sehested, M., and Nitiss, J.L. (2005). Stability of the topoisomerase II closed clamp conformation may influence DNA-stimulated ATP hydrolysis. J. Biol. Chem. *280*, 11920–11929.

Wigley, D.B., Davies, G.J., Dodson, E.J., Maxwell, A., and Dodson, G. (1991). Crystal structure of an amino-terminal fragment of the DNA gyrase B protein. Nature *351*, 624–629.

Williams, N.L., Howells, A.J., and Maxwell, A. (2001). Locking the ATP-operated clamp of DNA gyrase: probing the mechanism of strand passage. J. Mol. Biol. *306*, 969–984.

Winn, M.D., Isupov, M.N., and Murshudov, G.N. (2001). Use of TLS parameters to model anisotropic displacements in macromolecular refinement. Acta Crystallogr. D Biol. Crystallogr. *57*, 122–133.

Wittinghofer, A. (1997). Signaling mechanistics: aluminum fluoride for molecule of the year. Curr. Biol. *7*, R682–R685.

Yamada, S., Ono, T., Mizuno, A., and Nemoto, T.K. (2003). A hydrophobic segment within the C-terminal domain is essential for both client-binding and dimer formation of the HSP90-family molecular chaperone. Eur. J. Biochem. *270*, 146–154.

Accession Numbers

Coordinates and structure factors have been deposited in the RCSB protein data bank under accession numbers 1Z59 (ADP bound monomer), 1Z5A (ADP bound dimer), 1Z5B ($ADP{\cdot}AlF_4^-$ bound dimer), and 1Z5C ($ADP{\cdot}P_i$ bound dimer).

Supplemental Data

Structural Dissection of ATP Turnover

in the Prototypical GHL ATPase topo VI

Kevin D. Corbett and James M. Berger

Nucleotide-Mediated topoVI-B´ Dimerization Assay

To study the dimerization state of topoVI-B´ in solution in the presence or absence of nucleotide, we developed a glutaraldehyde-mediated cross-linking assay. TopoVI-B´ was diluted to 2 mg/mL in a buffer containing 20 mM HEPES pH 7.5, 400 mM NaCl, and 10% glycerol with 1 mM nucleotide (ADP, ATP, or AMP-PNP). The protein was incubated at 65°C for 10 minutes, followed by a slow cooling to room temperature (1°C/min). We next diluted the sample 8-fold in buffer and added glutaraldehyde to 0.025%. After 20 minutes, we removed 10 µL aliquots, quenched the cross-linking reaction with 5 µL 2M glycine, added 10 µL 2X SDS-PAGE loading dye, and ran 15 µL of each sample on an 8% SDS-PAGE gel (Supplemental Figure S2A). Monomer and dimer bands were quantified using ImageJ (Rasband, W.S., US National Institutes of Health, Bethesda, MD, http://rsb.info.nih.gov/ij/, 1997-2005), and the fraction of total protein present in the dimer band was calculated (Supplemental Figure S2B). We observe that ADP and ATP are most effective at mediating dimerization in solution under these conditions, and that virtually no dimer is detected in the absence of nucleotide.

Table S1. Data Collection, Refinement, and Stereochemistry

Data Collection	**ADP·AlF_4^- dimer**	**ADP·P_i dimer**	**ADP dimer**	**ADP monomer**
Resolution (Å)	30 – 2.0	30 – 2.2	30 – 2.2	30 – 2.1
Wavelength (Å)	1.116	1.100	1.000	1.100
Space Group	$P3_212$	$P3_212$	$P3_212$	$P2_12_12$
Unit Cell Dimensions (a, b, c) (Å)	74.08, 74.08, 344.38	74.50, 74.50, 346.46	74.57, 74.57, 345.56	94.57, 112.45, 56.08
I/σ (last shell)	20.1 (4.20)	23.4 (5.90)	15.0 (6.77)	12.1 (3.30)
[1] R_{sym} (last shell) (%)	0.060 (0.232)	0.059 (0.248)	0.084 (0.166)	0.100 (0.369)
Completeness (last shell) (%)	98.7 (98.9)	94.6 (97.3)	93.1 (84.0)	99.1 (99.9)
No. of reflections	547941	575703	1298763	282898
unique	72958	53646	52943	35386
Refinement				
Resolution (Å)	30 – 2.0	20 – 2.2	20 – 2.2	30 – 2.1

Number of reflections	69174	50547	50047	32440
working	65496	47857	47414	29524
free (% total)	3678 (5.0)	2690 (5.0)	2633 (5.0)	2916 (8.2)
[2]R_{work} (last shell) (%)	17.94 (20.0)	19.44 (21.7)	19.53 (19.4)	18.93 (22.3)
[2]R_{free} (last shell) (%)	20.80 (23.2)	23.22 (30.0)	23.09 (25.2)	22.76 (27.3)

Structure and Stereochemistry

Protein chains per AU	2	2	2	1
Number of atoms	7820	7699	7716	3894
protein	7454	7421	7452	3696
water	299	212	208	170
nucleotide	64	64	54	27
Mg^{2+}	3	2	2	1
r.m.s.d. bond lengths (Å)	0.012	0.015	0.014	0.020
r.m.s.d. bond angles (°)	1.102	1.364	1.196	1.171

[1]$R_{sym} = \Sigma\Sigma_j|I_j - \langle I\rangle|/\Sigma I_j$, where I_j is the intensity measurement for reflection j and $\langle I\rangle$ is the mean intensity for multiply recorded reflections.

[2]$R_{work,\ free} = \Sigma||F_{obs}| - |F_{calc}||/|F_{obs}|$, where the working and free *R*-factors are calculated using the working and free reflection sets, respectively. Free reflections were held aside throughout refinement.

Figure S1. The Active Site of topoVI-B´ is Buttressed on all Sides in the Dimerized State. Stereo view of the topoVI-B´ active site in the ADP-bound dimer state, showing the convergence of several structural elements that maintain the structure of the ATP lid in the presence or absence of a γ-phosphate moiety. The GHKL domain is shown in yellow, the transducer domain in orange, and dimer mate in gray. The side chains of residues 34, 38, 42, and 427 are shown as in Figure 2. The loop containing the ATP lid (residues 94-111) is shown in green, and the main-chain nitrogen atoms of the ATP lid are shown in blue. In addition, an ordered water in the γ-phosphate binding site is shown. Even without a γ-phosphate to engage the ATP lid, the structure of this loop is maintained through van der Waals, hydrophobic, and hydrogen bonding interactions from the transducer domain and the N-terminal strap of the dimer mate.

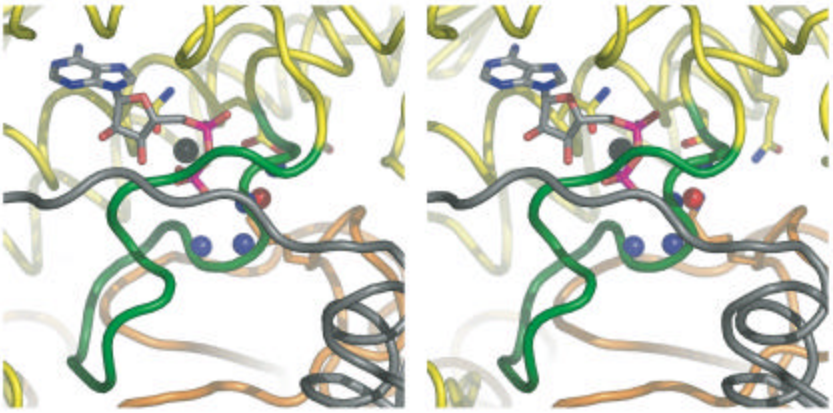

Figure S2. Dimerization of topoVI-B´ in Solution. (A) Gel showing glutaraldehyde-mediated cross-linking of dimerized topoVI-B´ in the presence of various nucleotides (AMP-PNP is labeled 'ANP'). The location of protein size markers are shown on the left, and the locations of monomer and dimer bands are shown on the right. (B) Quantitation of (A), showing the fraction of topoVI-B´ in the dimer band in the presence of various nucleotides. Each data point is an average of four independent measurements, and error bars represent standard deviations. Although some residual dimer species is detected in the absence of nucleotide, the band is diffuse and probably represents nonspecific background cross-linking.